Research Article | Vol. 32, No. 22 / 21 Oct 2024 / Optics Express 39924
Optics EXPRESS

# Optical fiber-coupled Kretschmann SPR sensor with re-attachable gold nano-thin film sensing chip

TEERAPAT RUTIRAWUT,[1,2] KWANJIRA JOONMASA,[1] AISSARA RASRITAT,[1] RATCHAPAK CHITAREE,[3] PANOMSAK MEEMON,[1,4] RAND ISMAEEL,[2,5] SORAWIS SANGTAWESIN,[1,4,6] AND WANVISA TALATAISONG[1,2,7]

[1]*School of Physics, Suranaree University of Technology, Nakhon Ratchasima 30000, Thailand*
[2]*Optoelectronics Research Centre, University of Southampton, Southampton, SO17 1BJ, UK*
[3]*Applied Optics Research Group, Department of Physics, Faculty of Science, Mahidol University, Bangkok 10800, Thailand*
[4]*Center of Excellence in Advanced Functional Materials, Suranaree University of Technology, Nakhon Ratchasima 30000, Thailand*
[5]*National Oceanography Centre, Southampton, SO14 3ZH, UK*
[6]*sorawis.s@g.sut.ac.th*
[7]*wanvisa.tala@sut.ac.th*

**Abstract:** We designed and demonstrated a portable and reusable surface plasmon resonance (SPR) sensor based on an optical fiber-coupled Kretschmann configuration with a variable detection limit enabled by the re-attachable gold nano-thin film. The prism angle of SPR has been optimized to 63.5 degrees to enable the SPR sensor to operate in the near-infrared band. We highlight the effects of the chromium to gold film thickness ratio and the prism angle on the SPR characteristics to improve sensitivity. Both simulations and experimental results reveal that the narrowest FWHM and deepest amplitude of the SPR curve were achieved when the chromium to gold film thickness ratio was set to 2 nm/40 nm. Furthermore, the refractive index (RI) sensitivity of the sensor was simulated within the RI detection range of 1.3235-1.3290, and with the optimized SPR sensor, we obtained a record high RI sensitivity of 34,888 nm/RIU. The capability to detect variations in saline and sucrose concentration in aqueous form has been experimentally demonstrated, revealing a sensitivity of 455 nm/M and 3,056 nm/M over concentration ranges of 0.10 to 0.55 M and 0.018 M to 0.053 M, respectively. The results show that the proposed optical fiber-coupled SPR sensor with an optimized sensing chip offers high sensitivity and is promising for a broad range of applications, including medical diagnostics, agriculture, food safety, and environmental monitoring. The sensor's advantages include miniaturization and flexibility, highlighting its potential for broad and versatile use.



## 1. Introduction

Surface Plasmon Resonance (SPR) is a highly sensitive optical technique for real-time detection of minute changes in the refractive index at metal-dielectric interfaces. It has found extensive applications in biomolecular interaction monitoring and analyte detection (chemical and biological) in liquid or gas environments [1–3]. This technique relies on the interaction between light and free electrons within a thin metallic layer, typically composed of a noble metal. At resonance, the incident light frequency aligns with the oscillation frequency of the electrons in the metal, leading to a significant energy transfer and thus the decrease in the reflected light intensity. This phenomenon signifies the generation of a surface plasmon wave through the transfer of photon

#538252 https://doi.org/10.1364/OE.538252
Journal © 2024 Received 20 Aug 2024; revised 2 Oct 2024; accepted 3 Oct 2024; published 17 Oct 2024

Optics EXPRESS

energy into the metallic layer. Due to their chemical stability and good sensitivity to refractive index changes, silver and gold are preferred metals for SPR [4–8].

Most SPR sensing devices are based on prism-coupling method. The conventional prism-coupled SPR sensor benefits from high stability, high sensitivity, real-time monitoring, and label-free detection. This type of SPR sensor offers a sensitive and label-free method to analyze interactions between biomolecules and ligands, making it suitable for biological and chemical sensing. Consequently, many commercialized SPR systems have demonstrated high biological and chemical sensitivity. However, these commercialized SPR devices are bulky due to the need for moving optics to vary the SPR angle, which is necessary to expand the dynamic range of the sensor for a wider range of refractive index analytes. As a result, they are limited to specific applications on a laboratory scale. Recently, the miniaturization of SPR sensors has gained considerable interest due to the growing need for real-time, in-situ monitoring in environmental, industrial processes, gas, food, biomedical, and healthcare applications.

Optical fiber sensors hold significant promise due to their unique advantages, such as immunity to electromagnetic interference, high sensitivity, and compact size. These features enable their integration into multi-fiber platforms for simultaneous detection of multiple compounds. Several reports detail the use of fiber optic techniques to create compact SPR sensor devices, including single mode fiber, photonic crystal fiber, nano/microfiber, and specialty fiber [9–14]. However, optical fiber based SPR sensors often involve complex fabrication processes, such as chemical etching, side polishing, or metallic material deposition along the fiber core. Additionally, the metallic sensing layer deposited on the optical fiber typically has a limited lifespan influenced by the operational environment. Harsh environments can significantly degrade the performance of optical fiber SPR sensors due to the deterioration of the metallic sensing layer, ultimately necessitating sensor disposal.

To enhance the stability, sensitivity, and compact size of SPR sensors, prism-based SPR has been integrated with optical fiber for sensing applications. This integration increases compactness and enables potential use in liquid environments. These works reveal the possibility and potential of creating an SPR sensor by integrating optical fiber with prism-based SPR sensors to achieve high stability, high sensitivity, and compact, in-situ monitoring capabilities for environmental applications [15–17].

In this paper, we have conducted simulations to optimize the prism angle for the Kretschmann SPR structure and determine the suitable thickness and ratio of the metal layer that provides the strongest resonance curve and narrowest FWHM. We propose and demonstrate a compact and high-sensitivity optical fiber-coupled Kretschmann SPR sensor with a simplified fabrication process and integrated changeable SPR sensing chips. The calculation results indicate that the maximum RI sensitivity can reach 34,888 nm/RIU within the RI range of 1.3235-1.3290. The proposed sensor can detect changes in the concentration of saline and sucrose solutions with sensitivities of 455 nm/M and 3,056 nm/M over concentration ranges of 0.10 to 0.55 M and 0.018 to 0.053 M, respectively. The novelty of this work lies in the design of the prism and optical fiber holder to create a compact optical fiber-coupled Kretschmann SPR sensor and the optimization of multilayer metal film thickness to provide a high-sensitivity SPR sensor. This structure leverages the sensitivity of the SPR sensor and the flexibility of optical fibers, which are key selling points.

## 2. Basic sensing principle of SPR sensor

The theoretical basis of surface plasmon resonance (SPR) is the interaction between an incident electromagnetic wave and the free electrons in a metal. Optical excitation of surface plasmons is carried out by means of the attenuated total reflection (ATR) method demonstrated by Otto and Kretschmann [18,19]. Based on an analysis of Maxwell's equation with appropriate boundary conditions, the wave vector for the surface plasmon wave () and evanescent wave vector of incident light ($k_{EW}$) that is parallel to the metal-sample interface can be expressed as $k_{sp} = \frac{2\pi}{\lambda_0}\sqrt{\frac{\varepsilon_m\varepsilon_s}{\varepsilon_m+\varepsilon_s}}$

Optics EXPRESS

and $k_{EW} = \frac{2\pi}{\lambda_0}\sqrt{\varepsilon_p}\sin\theta$, respectively [20], where $\lambda_0$ is the wavelength of light in a vacuum, $\varepsilon_p$ is dielectric constant of prism, and $\theta$ is angle of incident. $\varepsilon_m = \varepsilon_m' + i\varepsilon_m''$ and $\varepsilon_s = \varepsilon_s' + i\varepsilon_s''$ are the complex dielectric constants of the metal and the sample layer, respectively.

At a specific incident angle and with a wavelength dependence of $\varepsilon_m$, the evanescent wave vector ($k_{EW}$) matches that of the wave vector of SPW ($k_{sp}$), i.e., $k_{sp} = k_{EW}$, and the SPR behavior occurs. The energy of the incident light will be partially transferred to the SPW, resulting in a sharp drop in the energy of the reflected light. This resonance angle ($\theta_{SPR}$) can be described as follows:

$$\theta_{SPR} = \sin^{-1}\sqrt{\frac{\varepsilon_m\varepsilon_s}{\varepsilon_p(\varepsilon_m+\varepsilon_s)}} \quad . \tag{1}$$

The reflectivity of the multilayer based on Kretschmann coupling configuration can be derived from a combination of Fresnel equations and interference theory. The intensity and phase of the reflected p-polarized light can be determined using the complex reflection coefficient of the multilayer medium structure which can be expressed as [21]:

$$R^p = |r_l^p|^2 \quad , \tag{2}$$

$$r_l^p = \frac{r_{l-1,l}^p + r_{l+1}^p e^{2it_l k_{l\perp}}}{1 + r_{l-1,l}^p r_{l+1}^p e^{2it_l k_{l\perp}}}; l = 1,\ 2,\ \ldots.,s \quad , \tag{3}$$

where $t_l$ represents the thickness of the $l^{\text{th}}$-layer, $\varepsilon_l$ is the dielectric constant of the $l^{\text{th}}$-layer, $k_{l\perp}$ is the orthogonal component (to the metal-sample interface) of wave vector of the incident light in the $l^{\text{th}}$ layer, and $c$ presents the speed of light in vacuum. Equations (2), (3) reveal that the reflection coefficient ($r_l^p$) can be determined by the dielectric constant of each layer and the metal film thickness.

## 3. Modelling and simulation results

### 3.1. Simulation of the layer thicknesses

To demonstrate the SPR principle of the sensor, the simulation was conducted to optimize an appropriate incident angle, which is related to the prism angle, to achieve the SPR spectra within the desired range of wavelength. The relationship of the composite films with the resonance angle can be calculated using Eq. (1). In the simulation, the film thickness of chromium (Cr) and the gold (Au) is initially set to 5 nm and 45 nm, respectively [22]. Water was chosen as the sample layer to imitate the refractive index of an aqueous environment.

The SPR sensor's performance is influenced by the material choice of metal film. Metals used in SPR applications must possess sufficient free electron density or conductivity to interact with electromagnetic waves and generate a plasmonic field. However, not all metals are suitable for SPR-based sensor applications; for instance, highly reactive metals like sodium (Na) and costly indium (In) are not preferred. Additionally, metals such as silver (Ag), copper (Cu), and aluminum (Al) are highly susceptible to oxidation [23]. Copper, the second most conductive material after aluminum, shares a similar attenuation rate to gold (Au). Nonetheless, Cu susceptibility to oxidation diminishes its attractiveness for researchers compared to Au [24]. In this work, Au was chosen since it is well-known as an excellent material for SPR sensors.

In order to evaluate the theoretical reflection characteristics of the Kretschmann SPR as presented in Fig. 1(a), simulation using the finite difference time domain method (with the commercial FDTD solver, Lumerical© STACK Optical Solver) were performed on a multilayer stack instead of direct calculations of Maxwell's equations. The command from STACK optical solver calculates the reflection and transmission of a plane wave through an arbitrary multilayer stack using the analytic transfer matrix method. This function returns the fraction of transmitted and reflected power ($T_s$, $T_p$, $R_s$, $R_p$), and the complex reflection and transmission coefficients ($t_s$, $t_p$,

Optics EXPRESS

$r_s$, $r_p$) for both S and P polarizations. The results in Fig. 1(b) and (c) show that when considering the resonance wavelength of SPR spectra is blue-shifted as the incident angle increases, owing to the wavelength-dependent of dielectric constants (see Eq. (1)). To confirm the simulation results, the SPR angle within the wavelength range of 1,000–1,600 nm were calculated by using Eq. (1), the result showing that at the wavelength of 1,000 nm and 1,600 nm, the SPR angle is 64.0 and 62.2 degrees, respectively which is correspond with the simulation result in Fig. 1(b) and (c).

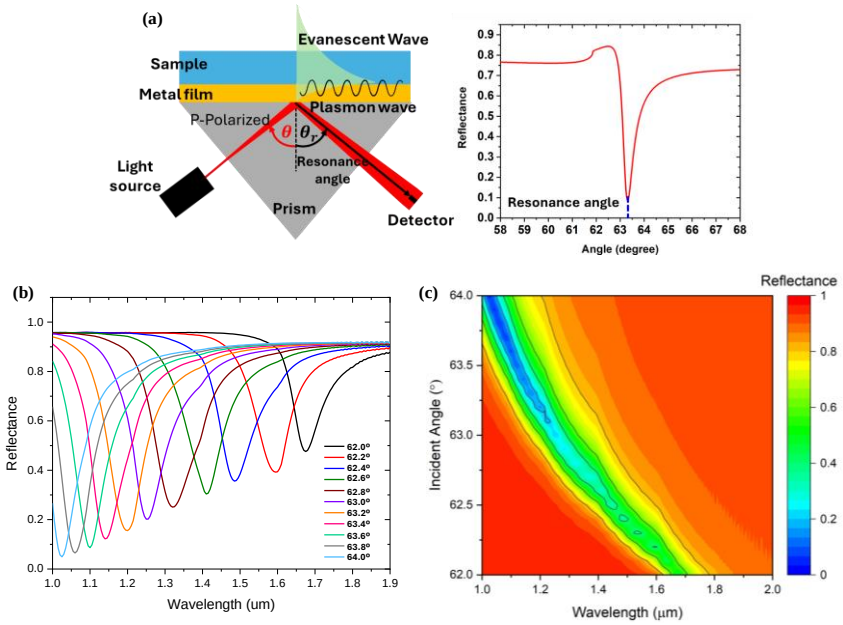


**Fig. 1.** (a) Schematic of a Kretschmann configuration based SPR sensor showing the low power of the reflected light at the resonance angle. (b) Simulation results of the reflectance of SPR spectra as a function of wavelength with the variation of incident angle between BK7 and Au film medium. (c) Contour plot showing the reflectance from the SPR system at different incident angles and wavelengths.

Due to the characteristics of the broadband light source used in this work, which has a high-power operating wavelength starting at around 1,100 nm, an incident angle of 63.5° was chosen to operate the SPR sensor in the range of 1,100–1,600 nm. This wavelength range was also chosen to enhance the sensitivity of the SPR sensor compared with the visible range as the longer wavelength provides higher sensitivity [25]. The devices used in this work including the polarization maintaining fiber and GRIN lenses are designed for the telecom-wavelengths.

### *3.2. Simulation for intensity interrogation*

The thickness of the Au film defines the resonance conditions and the performance of the SPR sensor [26]. When the resonance condition is fulfilled, a dip at a particular wavelength is observed in each SPR spectra, known as the resonance wavelength. To deposit the Au film on the amorphous substrate such as the BK7 used in this research, chromium (Cr) will be generally used as an adhesive layer to ensure firm contact between the metallic layer and the prism. Therefore, a very thin layer (< 10 nm) of Cr film will be deposited before the Au deposition. Past studies have shown that the thickness of Au film directly affected the resonance conditions: SPR resonance wavelength and full width at half-maximum (FWHM) of the SPR spectra. Although the effect of the adhesion layer to the optical properties of the device can be ignored for most applications,

Optics EXPRESS

it significantly impacts the near-field response of plasmonic sensors at the plasmon resonance. However, detailed understanding is still lacking concerning the effect of Cr thickness and the dependency of Cr thickness and metal film thickness on the resonance condition.

In this work, we studied the effect of the Cr film thickness on the performance of the SPR, especially for sensing applications. A four-layer stack of materials from bottom to top, including BK7 prism, Cr, Au, and water, was used in the simulation. To study the effect of Cr to the SPR spectra, Cr thickness varied from 1 nm to 10 nm in 1 nm increments. The results in Fig. 2(a) show that the thinnest Cr layer (1 nm) provides the deepest dip and narrowest FHWM of the resonance. An increase in Cr thickness from 1 nm to 2 nm results in a decrease in the SPR depth by approximately two orders of magnitude. Furthermore, when the Cr film thickness increases from 1 nm to 10 nm, the reflectance of the SPR dip gradually increases. As the dip at a resonance wavelength of SPR spectra corresponds to the resonance between the incident electromagnetic wave and the plasmon wave on metal surface, lower reflectance of the SPR dip indicates a stronger resonance. Based on the simulation results, the Cr thin film with a thickness of 1 nm provides the pronounced resonance, making them ideal candidates for highly sensitive sensing applications. This is because the Cr is a poor plasmonic material resulting in high optical losses. Moreover, its placement at the Au/dielectric interface would position Cr at the location of the largest optical fields. Therefore, the increasing of Cr layer which has a poor plasmonic metal results in a large decrease in the propagation distance of the plasmon wave. Thus, the thicker Cr interface layer leads to shallower SPR dip depth. However, in practice, depositing a thin film with 1 nm precision is challenging to control due to equipment limitations, and a very thin adhesive layer can cause poor adhesion between the substrate and the metal film. Therefore, the Cr with thickness of 2 nm was chosen for this research as it provides the deepest SPR dip with a narrower FWHM compared to thicker Cr layer.

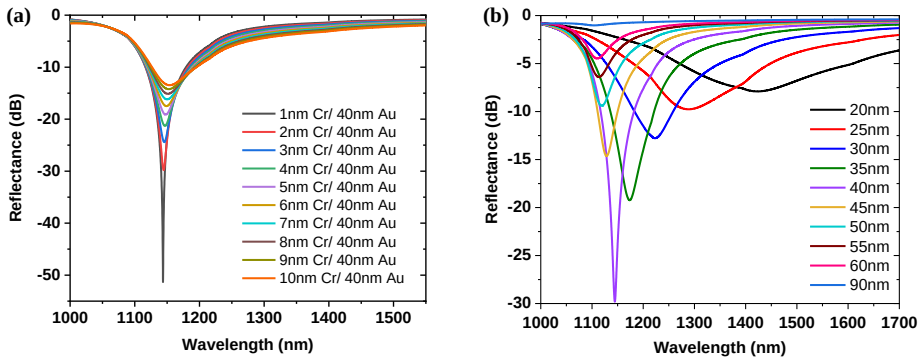


**Fig. 2.** Simulation results showing the effect of the Cr layer thickness on Au metal based SPR resonance spectra when the thickness of Cr varied from 1 to 10 nm with 1 nm increments. (b) Effect of the Au film thickness on the SPR resonance spectra when the Cr thickness was fixed at 2 nm and the Au thickness varied from 20 to 90 nm.

The effect of Au film thickness on the SPR spectra was also studied by setting the thickness of Cr layer to 2 nm. Figure 2(b) reveals the relationship between the SPR resonance spectrum and the thickness of Au layer from 20 nm to 90 nm in 5 nm increments. As the Au film thickness increases from 20 nm to 90 nm, the SPR spectra gradually blue-shift, and the SPR dip depth increases until the Au thickness reaches 40 nm. Then, the SPR dip depth starts to decrease when the Au thickness exceeds 40 nm. The variation in a dip of SPR depth (reflectance) and FWHM is owing to the coupling between the incident electromagnetic wave and the plasmon wave, which is related to the thickness of the Au film. A very thin Au film leads to high loss and low coupling between the electromagnetic wave and the plasmon wave due to the small amount of the electron

Optics EXPRESS

in the thin Au film. Conversely, the evanescent wave of incident light can hardly penetrate a very thick Au film (thickness >45 nm), leading to poor interaction between the electromagnetic wave and the plasmon wave. At a thick Au film, the SPR excitation became less efficient due to the electron absorption by the metal itself, thus inhibiting the SPR effect. The Au film with a thickness of 40 nm shows the deepest and narrowest SPR dip, indicating high performance of the SPR sensor.

The sensitivity ($S$) and figure of merits (FOM) values of the sensor, which are directly related to determining the performance of the sensor, can be calculated according to the formulas given below [27]:

$$S = \frac{\Delta\lambda}{\Delta n}, \tag{4}$$

$$FOM = \frac{\mathrm{S}}{\mathrm{FWHM}}, \tag{5}$$

where $\Delta\lambda$ corresponds to the shift in the resonance wavelength and $\Delta n$ is the change in the refractive index of the sample.

Regarding Eq. (4) and (5), the higher sensitivity and smaller FWHM lead to higher accuracy and FOM, resulting in high sensitivity performance of the sensor. Thus, to achieve a high sensitivity SPR sensor, Au film with a thickness of 40 nm appears to be an optimal thickness. Therefore, in this research, a 2 nm Cr and 40 nm Au multilayer is the optimal design to obtain the best trade-off between sensitivity and FOM of the sensor.

Next, the sensing performance of the sensor based on the optimal structure was simulated, and the results are shown in Fig. 3, where (a) shows the transmission spectra of the sensor at different sample refractive indies (RIs) from 1.3235-1.3290. The simulation results show that the SPR resonance wavelength is increased with the increasing of the sample RI. The RI sensitivity of the optimized SPR sensor was calculated (using Eq. (4)) to be 34,888 nm/RIU as presented in Fig. 3(b). The calculation of the RI sensitivity from the simulation result based on the optimized angle of prism and the thickness of Cr and Au film showing that the SPR sensor can provide a high RI sensitivity of 34,888 nm/RIU.

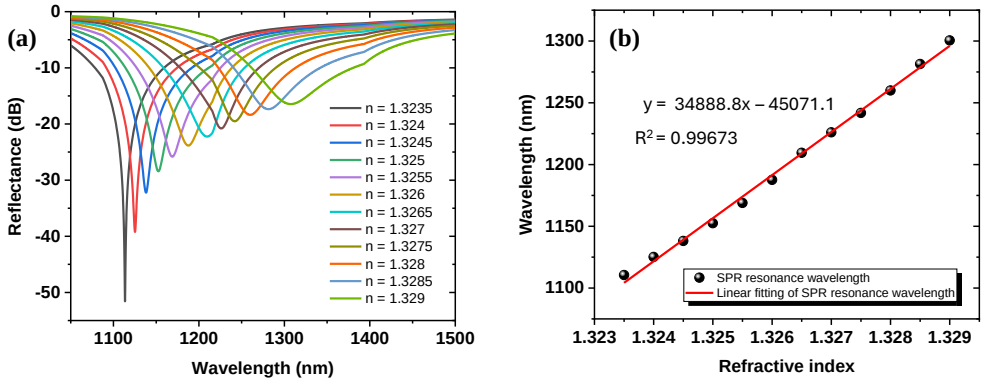


**Fig. 3.** (a) Simulation result of the RI sensing performance of the optimized SPR sensor. (b) The relationship between the SPR resonance wavelength from the simulation and the refractive index of the sample, displaying linearly fitted data with a sensitivity of 34,888 nm/RIU.

## 4. Optical fiber coupled SPR sensor structure

The proposed optical fiber coupled SPR sensor is illustrated in Fig. 4 (a-b) This optimized incident angle of 63.5° was used to design the prism for the SPR setup, as illustrated in Fig. 4(a). A

Optics EXPRESS

white light source from a supercontinuum laser (SuperK EXTREME (EXU-6), NKT Photonics) was used, along with a polarization maintaining (PM) optical fiber collimator, to guide the light beam to a prism. Due to the unpolarized nature of the light from super continuum source, the PM fiber was used together with the polarization controller to tune the polarization of the input light of the SPR system to be P-polarization. To ensure that the input light from the PM fiber is P-polarized when entering the SPR system, the slow axis of the PM fiber (panda) is aligned parallel to the plane of incidence. The SPR spectrum is monitored in real-time as the input light's polarization is adjusted using the polarization controller, as illustrated in Fig. 2. The deepest dip in the SPR spectrum occurs when the input light is P-polarized. The PM fiber collimator used in this research features a 1.8 mm diameter GRIN lenses, a working distance of 15± 5 cm, and a beam diameter of ≤ 0.5 mm (50-1550PM-FC, Thorlabs, USA). The prism used in this research is a BK7 glass prism with a prism angle of 53° and the other two corners of prism have an angle of 63.5°, as presented in Fig. 4(a). A re-attachable chromium (Cr) and gold (Au) nano-film SPR sensing chip, with Cr and Au thicknesses of 2 nm and 40 nm, respectively, was deposited onto a 5 mm × 5 mm × 0.1 mm BK7 coverslip using an e-beam evaporation system. A single-mode optical fiber collimator with the same specifications as the PM fiber collimator was used to collect the reflected light from the prism. Then, the output signal from the single-mode optical fiber collimator was delivered to the optical spectrum analyzer (AQ6370D, Yokogawa, Japan).

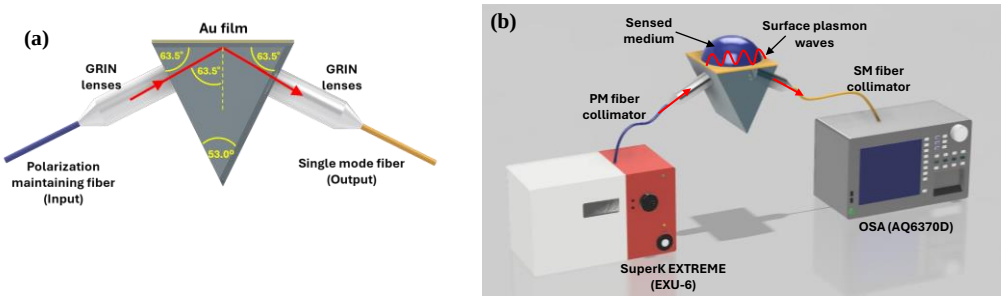


**Fig. 4.** (a) Schematic of the prism design based on the simulation result for the proposed optical fiber-coupled Kretschmann SPR sensor. (b) The proposed optical fiber-coupled Kretschmann SPR sensing system, including the supercontinuum light source and the optical spectrum analyzer.

To confirm the thickness of the metal film deposited on the BK7 cover slip, the step height of the Cr - Au film on the chip was measured with an atomic force microscope (AFM) (NX10, Park System), operating in true non-contact mode using a silicon tip. The AFM analysis, conducted over a $90 \times 20$ μm$^2$ area, revealed an average step height of 41.9 nm for the Cr - Au film, as illustrated in Fig. 5. Although, the sample exhibited nearly uniform morphology, some molecular clusters were present. These clusters, which occurred during the preparation of the thin film, caused some high hills in certain areas. The smoother surface roughness of metal film results in stronger coupling between the electromagnetic wave and plasmon wave. Thus, the roughness of the surfaces of the metal depositions has been preliminarily analyzed by using the same AFM instrument. The scans have been realized in non-contact mode using a silicon tip with a spring constant of 37 N/m and a typical cantilever tip radius ROD of 6 nm. The typical surface root mean square (RMS) roughness, evaluated on extended regions of 1800 μm$^2$, is of the order of 4.9 nm. These values of RMS roughness are typical of metal depositions over glass substrates.

To assemble the proposed optical fiber-coupled Kretschmann SPR structure, the prism and optical fiber collimator holder were designed and created using a 3D printer with polylactide (PLA) material. Based on the specification of the fiber collimator with a beam diameter of ≤ 0.5 mm, a misalignment of 1.0 mm can cause more than 50% coupling loss. Thus, the holder

Optics EXPRESS

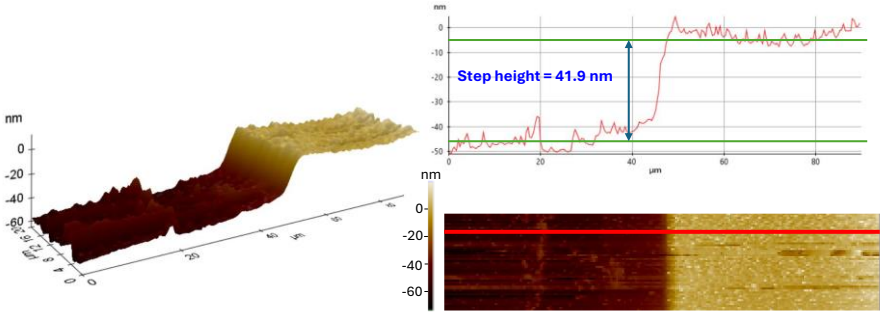


**Fig. 5.** Step height of Cr + Au film on the BK7 cover slip measured by AFM showing the step height of 41.9 nm.

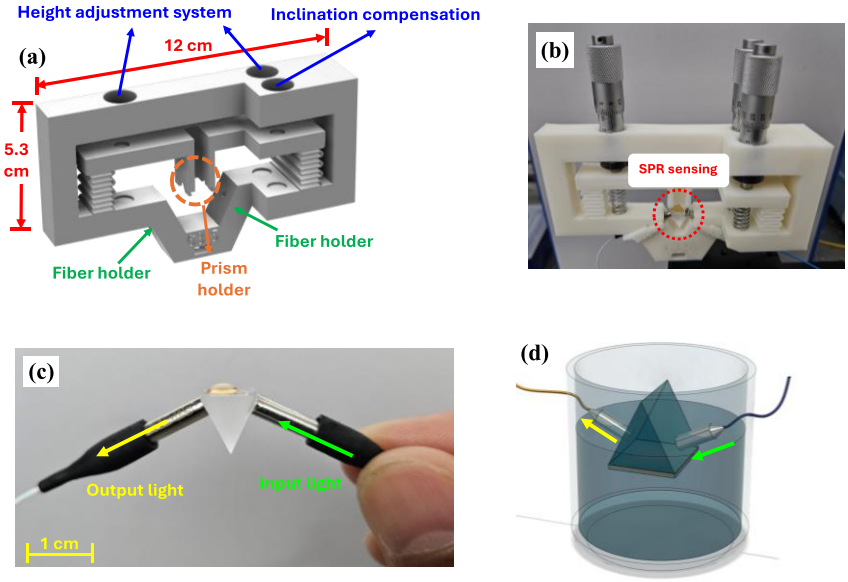


**Fig. 6.** (a) A 3D model design of the prism and optical fiber collimator holder used for aligning the input and output fibers with 3 degrees of freedom adjustment. (b) Photographs of the experimental setup to test and manufacture the optical fiber-coupled Kretschmann SPR sensor based on wavelength detection. (c) A compact optical fiber-coupled Kretschmann SPR sensor. (d) Experimental setup to demonstrate the concentration sensitivity of the proposed sensor for saline and sucrose solution.

was designed to precisely align the input and output optical fiber collimators with the prism. As demonstrated in Fig. 6(a), the holder was designed to integrate three micrometers. Two micrometers were used to adjust the height and the left-right tilt of the prism to match the reflection plane. In addition, the other micrometer, facing the front of the holder, was used to adjust the front-back tilt of the prism. Moreover, this holder design combines the 3D-printed springs with real springs to increase the flexibility of the prism height adjustment. Due to the unpolarized nature of the broadband light source, a polarization controller was added between the light source and the SPR system to ensure the polarization of the input signal is P-polarized. A photograph of the developed optical fiber-coupled Kretschmann SPR system in Fig. 6(b) shows the entire sensing system.

Optics EXPRESS

In the experiment, the custom-made prism had an isosceles triangular base with angles of 53°, 63.5°, and 63.5°, corresponding to a base size of 10 mm ×10 mm × 8.92 mm and a height of 10 mm. The BK7 coverslip with an Au thin film with a total thickness of ~ 42 nm (SPR sensing chip), was attached to the 8.92 mm side of the prism using matching index liquid (IML 150, Edmund: Norland). The collimated P-polarized optical signal, emerging from the fiber collimator lens, strikes the SPR sensing chip at an angle of 63.5°, which is greater than the angle for TIR (see Fig. 4(a)). After reflecting off the SPR sensing chip, the beam is coupled through the output collimating lens into the optical fiber.

To ensure the maximum coupling between the input light and the output light through the optical fiber collimator, the optical fiber-coupled Kretschmann SPR sensing system was tested on the holder by dropping the deionized (DI) water onto the sensing chip. Then, the holder has been adjusted, and the SPR signal was monitored until the maximum coupling is achieved. A compact optical fiber-coupled Kretschmann SPR sensing device was assembled by gluing the optical fiber collimator on the side of the prism as shown in Fig. 6(c). The sensing chip was encapsulated to ensure the stable attachment with the prism before using it as a sensor for the aqueous solution (Fig. 6(d)).

## 5. Optical fiber-coupled Kretschmann SPR sensor characterizations and discussions

When the SPR Au sensing chip is exposed to an aqueous solution, the light source launched into the prism produces an evanescent field that excites a surface plasmon wave at the metal-prism interface, resulting in the attenuation of the reflected signal. As the incident angle of the input light is fixed by the angle of the prism, the coupling of the evanescent optical field into the generated surface plasmon wave strongly depends on the wavelength of the input optical signal, the sample refractive index, the ambient temperature, and the metallic layer properties (thickness, pattern, etc.). The spectral reflectance of the SPR sensor is then evaluated by an optical spectrum analyzer (OSA) at the monitoring end.

Figure 7(a) shows the experimental result of the SPR spectra when DI water was dropped on the sensing chip. The resonance wavelength is located at 1,117 nm, which is 27 nm different from the calculated resonance wavelength of 1,144 nm. This discrepancy can be attributed to misalignment between the sensing chip and the prism, as the chip floats on the matching index liquid, causing a deviation in the incident angle at the prism-Au interface. A 0.1° difference in the incident angle leads to a change in resonance wavelength of approximately 25 nm. Moreover, the difference in the depth of the SPR dip at the resonance wavelength between the experimental and calculated results is caused by the quality of the metal film. Smoother surface roughness results in stronger coupling between the electromagnetic wave and the plasmon wave, leading to a deeper SPR dip. Therefore, improving the metal film's surface roughness can enhance the depth of the SPR dip at the resonance wavelength.

To demonstrate the concept of a compact optical fiber-coupled Kretschmann SPR sensor, the RI detection performance of the sensor was investigated using saline and sucrose solutions. The saline solution was prepared by dissolving NaCl in DI water at different concentrations ranging from 0.10 to 0.55 mol/L (M). Based on the calculation of RI sensitivity in Fig. 3(a-b), the RI detection range of the proposed SPR sensor is RI = 1.3235-1.3290. Thus, the saline concentration of 0.10 to 0.55 M was used to fit within the RI detection range of the sensor.

In the experiments, the sensor was immersed in saline solutions of different concentrations, and the SPR spectra were recorded for each concentration. The SPR spectra with different concentrations of saline solution are illustrated in Fig. 7(b). The results show that the resonance wavelength of SPR spectra increases with an increase in saline concentration. The sensitivity of the sensing device was analyzed by fitting the resonance wavelength of the SPR dip at each saline concentration. An asymmetric SPR sensor response curve-fitting equation was used to determine

Optics EXPRESS

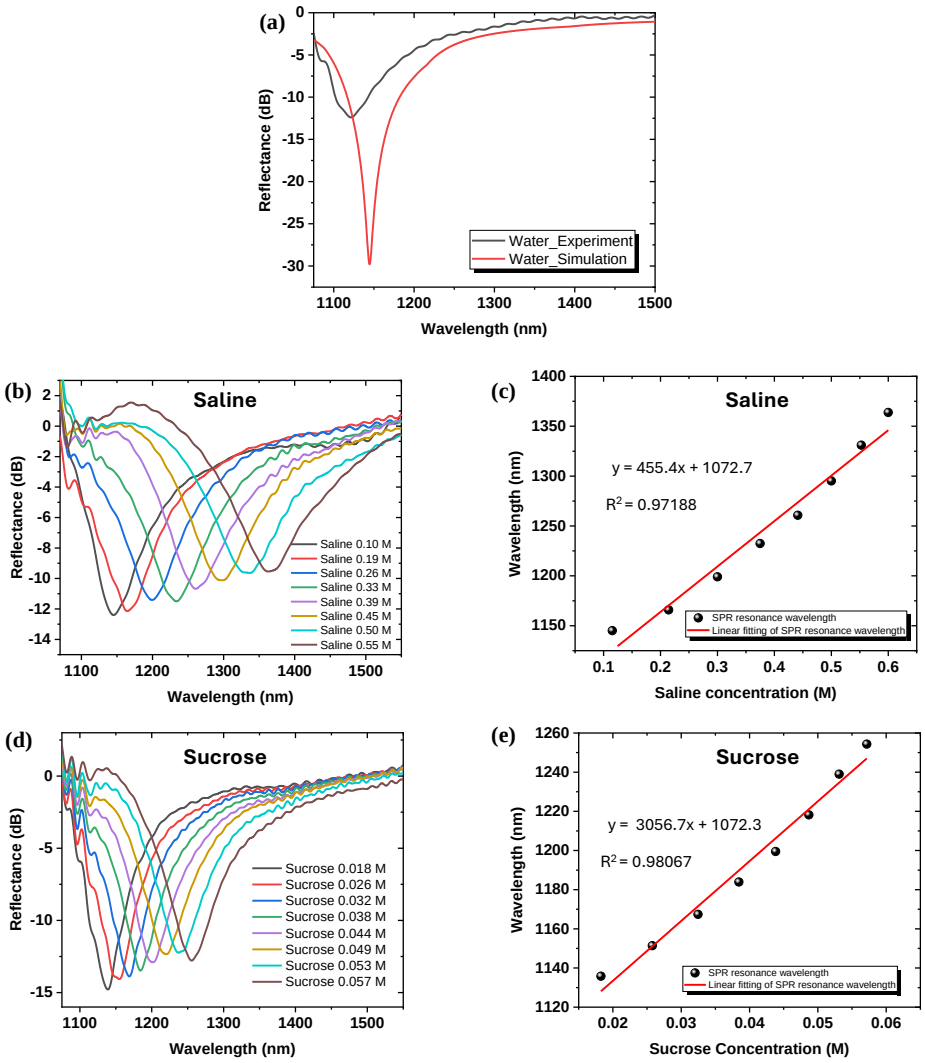


**Fig. 7.** The SPR reflectance as a function of wavelength for (a) DI water and (b) the saline solution (NaCl) at various concentrations. (c) The relationship between the SPR resonance wavelength and saline concentration, showing linearly fitted data with a sensitivity of 455 nm/M. (d) The SPR reflectance as a function of wavelength for sucrose solution. (e) The relationship between the SPR resonance wavelength and saline concentration, showing linearly fitted data with a sensitivity of 3056 nm/M.

the SPR resonance wavelength [28]. The results in Fig. 7(c) reveal the spectral response at different saline concentrations. By fitting the wavelength dip and the saline concentration with a linear fit, a slope of 455±31 nm/M was calculated with an $R^2$ of 0.97188.

To further evaluate the performance of the proposed SPR sensor, sucrose solutions were also used to determine the sensor's sensitivity. The sucrose solution was prepared by dissolving sucrose in DI water at different concentrations that match the RI detection range of the proposed SPR sensor of 1.3235-1.3290. Thus, the sucrose concentration of 0.018 M - 0.053 M was used in this experiment. The sensor was immersed in the sucrose solutions of different concentrations, and the SPR spectra for each concentration are presented in Fig. 7(d). The concentration

Optics EXPRESS

sensitivity of the sensor was analyzed using the same method as for the saline concentration. The results in Fig. 7(e) reveal the spectral response at different sucrose concentrations and the linear fitting provides the sucrose concentration sensitivity of 3056±175 nm/M with an $R^2$ of 0.98067.

The limit of detection (LOD) of the proposed sensor can be calculated by using the equation: $\text{LOD} = \frac{\Delta\lambda}{S}$ where $\Delta\lambda$ denotes the spectrometer's wavelength resolution and S indicates the sensor's sensitivity. When the wavelength resolution of the spectrometer is 0.1 nm are $2.2 \times 10^{-4}$ $M^{-1}$ and $3.3 \times 10^{-5}$ $M^{-1}$ for saline and sucrose solution respectively.

Subsequently, the temperature detection performance of the sensor was investigated. The sensor was immersed in DI water. The different temperature was applied to the DI water by using the hot plate. So that the temperature was varied in the range of 10-45 °C, and the thermocouple was placed next to the sensor to ensure the accurate temperature that applied to the sensor. The transmission spectra were recorded every 5 °C. The experimental result in Fig. 8(a) showing that the SPR wavelength is decreased with the increase of temperature. The fitted relationship between temperature and resonance wavelength is shown in Fig. 8(b) which reveals the temperature sensitivity of 1.00 ± 0.04 nm/°C with an $R^2$ of 0.98393. The low temperature sensitivity of the sensor can be used to be the background sensitivity of the sensor when working in real environments.

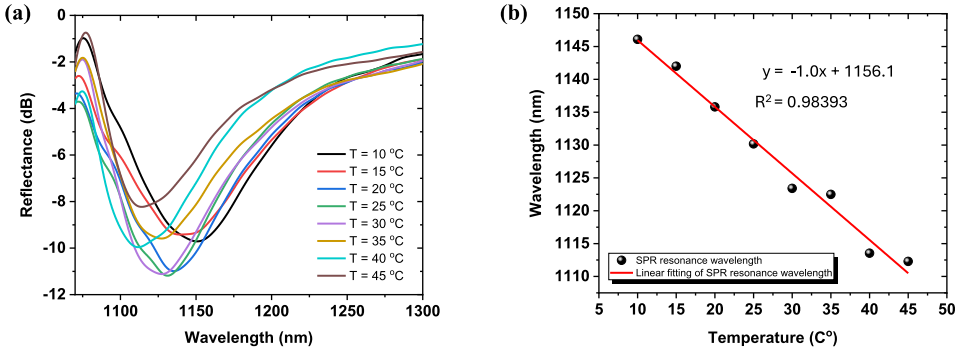


**Fig. 8.** (a) Experimental results of temperature sensing performance of the sensor. (b) The relationship between the SPR resonance wavelength and ambient temperature, showing linearly fitted data with a sensitivity of 1 nm/°C.

Above are the performance metrics of the sensor, which we compared with the recently published optical fiber SPR sensors. It can be seen from Table 1 that the proposed SPR sensor outperforms the other optical fiber-based SPR sensors.

In comparison to other optical fiber-based SPR sensors, the proposed sensor offers numerous advantages. Firstly, it employs compact size with disposable sensing chips, enabling its utilization as a platform for remotely sensing and measuring various compounds with diverse sensing chips. Secondly, while conventional optical fiber SPR sensors possess a restricted measurement range, the proposed sensor features a broad and customizable measurement range, determined by the chosen chip substrate material. By elevating the refractive index of the substrate, a wider measurement range can be achieved. Thirdly, the sensitivity of the proposed sensor can be controlled by the refractive index of the selected substrate on the sensor chip and the wavelength of the light source. Fourthly, by using the proposed SPR sensing system, motorized stages used for conventional SPR systems are not needed. As the stability of the conventional SPR system is based on the stability of the motorized stages, which is the most expensive part, the system demonstrated in this manuscript does not require any scanning system. Hence, it can offer more reliable stability with a compact size. Consequently, the sensor exhibits very high sensitivity compared to the conventional SPR sensors. These distinctive characteristics make

Optics EXPRESS

**Table 1. Performance comparison of the proposed fiber-coupled Kretschmann SPR sensor with other SPR sensors**

| Sensing structure | Target Analyte | Sensitivity | Wavelength | Year | Reference |
|---|---|---|---|---|---|
| SPR based Polymer-tipped optical fiber (PTOF) coated with a gold film and a Barium Titanate ($BaTiO_3$) | RI range: 1.33-1.34 | 6,710 nm/RIU | 800–1,400 nm | 2019 | [29] |
| SPR and PCF | RI range: 1.33-1.37 | 13,000 nm/RIU | 500–1,100 nm | 2020 | [30] |
| SPR PCF/Ag nanowires | RI range: 1.32-1.38 | 10,286 nm/RIU | 700–1,200 nm | 2020 | [31] |
| SPR PCF/Au layer | RI range: 1.3323-1.3359 | 13,592 nm/RIU | 500–1,000 nm | 2020 | [32] |
| SPR and dual-core D-Formed PCF | RI range: 1.40-1.45 | 18,800 nm/RIU | 500–1,100 nm | 2022 | [33] |
| This work | RI range: 1.3235-1.3290 | 34,888 nm/RIU | 1,000–1,550 nm | 2024 | - |

the proposed optical fiber-coupled Kretschmann SPR sensor particularly suitable for various sensing applications in remote area, including environmental monitoring and the detection of Greenhouse gas in aqueous or Greenhouse gas in deep ocean.

## 6. Conclusions

In this work, we propose and experimentally demonstrate a novel compact and flexible dynamic range optical fiber-coupled Kretschmann SPR device featuring a re-attachable gold nano-thin film SPR sensing chip. Intensive simulations were conducted to optimize dependency of Cr layer thickness on Au metal based SPR, illustrating the conditions necessary for achieving high depth with a small FWHM of the SPR spectra, resulting in high sensor sensitivity. The sensor exhibited a high RI sensitivity of 34,888 nm/RIU within the RI range of 1.3235-1.3290.

Experimental demonstrations showed the sensor's capability to detect variations in saline and sucrose concentrations in aqueous form, revealing sensitivities of 455 nm/M and 3,056 nm/M over concentration ranges of 0.10 to 0.55 M and 0.018 to 0.053 M, respectively. This is the first demonstration of a compact and flexible SPR sensor. The developed sensing system has shown precise alignment of the input and output fiber collimators with the prism, indicating potential for packaging the SPR sensing head for waterproof operation in the future.

**Funding.** NSRF via the Program Management Unit for Human Resources & Institutional Development, Research, and Innovation (B13F660057); Optica Foundation (20th Anniversary Challenge program).

**Acknowledgments.** T. Rutirawut and S. Sangtawesin acknowledge the financial support from the NSRF via the Program Management Unit for Human Resources & Institutional Development, Research, and Innovation [grant number B13F660057]. W. Talataisong gratefully acknowledges the funding support from the Optica foundation via the Optica Foundation 20th Anniversary Challenge program. We acknowledge Microelectronics Technology Development Section, Technical and Engineering Development Division, SLRI for thin film coating.

**Disclosures.** The authors declare no conflicts of interest.

**Data availability.** Data underlying the results presented in this paper are not publicly available at this time but may be obtained from the authors upon reasonable request.

Optics EXPRESS

## References


1. J. Homola, S. S. Yee, and G. Gauglitz, "Surface plasmon resonance sensors: review," Sens. Actuators, B **54**(1-2), 3–15 (1999).
2. M. D. Baiad and R. Kashyap, "Concatenation of surface plasmon resonance sensors in a single optical fiber using tilted fiber Bragg gratings," Opt. Lett. **40**(1), 115–118 (2015).
3. L. Liu, Z. Liu, Y. Zhang, *et al.*, "V-shaped micro-structure optical fiber surface plasmon resonance sensor for the simultaneous measurement of the refractive index and temperature," Opt. Lett. **44**(20), 5093–5096 (2019).
4. S. A. Zynio, A. V. Samoylov, E. R. Surovtseva, *et al.*, "Bimetallic Layers Increase Sensitivity of Affinity Sensors Based on Surface Plasmon Resonance," Sensors **2**(2), 62–70 (2002).
5. P. Lecaruyer, M. Canva, and J. Rolland, "Metallic film optimization in a surface plasmon resonance biosensor by the extended Rouard method," Appl. Opt. **46**(12), 2361–2369 (2007).
6. C. Perrotton, N. Javahiraly, M. Slaman, *et al.*, "Fiber optic surface plasmon resonance sensor based on wavelength modulation for hydrogen sensing," Opt. Express **19**(S6), A1175–A1183 (2011).
7. J. Hottin, E. Wijaya, L. Hay, *et al.*, "Comparison of Gold and Silver/Gold Bimetallic Surface for Highly Sensitive Near-infrared SPR Sensor at 1550 nm," Plasmonics **8**(2), 619–624 (2013).
8. D. V. Nesterenko and Z. Sekkat, "Resolution Estimation of the Au, Ag, Cu, and Al Single- and Double-Layer Surface Plasmon Sensors in the Ultraviolet, Visible, and Infrared Regions," Plasmonics **8**(4), 1585–1595 (2013).
9. Ó Esteban, M. Cruz-Navarret, A. González-Cano, *et al.*, "Measurement of the degree of salinity of water with a fiber-optic sensor," Appl. Opt. **38**(25), 5267–5271 (1999).
10. D. J. Gentleman and K. S. Booksh, "Determining salinity using a multimode fiber optic surface plasmon resonance dip-probe," Talanta **68**(3), 504–515 (2006).
11. T. T. Nguyen, E. C. Lee, and H. Ju, "Bimetal coated optical fiber sensors based on surface plasmon resonance induced change in birefringence and intensity," Opt. Express **22**(5), 5590–5598 (2014).
12. Z. Yin and X. Jing, "Experimental Study of Surface Plasmon Resonance Refractive Index Sensor Based on Side-Polished Few-Mode Fiber," IEEE Trans. Instrum. Meas. **72**, 1–6 (2023).
13. Z. Yin and X. Jing, "Visible-NIR surface plasmon resonance sensing technology for high precision refractive index detection," Opt. Lett. **49**(6), 1477–1480 (2024).
14. Z. Yin, X. Jing, K. Li, *et al.*, "Cascaded dual-channel broadband SPR fiber optic sensor based on Ag and Ag/ZnO/PDMS film structure," Opt. Express **32**(4), 6190–6203 (2024).
15. P. Preechaburana, M. C. Gonzalez, A. Suska, *et al.*, "Surface Plasmon Resonance Chemical Sensing on Cell Phones," Angew. Chem., Int. Ed. **51**(46), 11585–11588 (2012).
16. Y. Liu, Q. Liu, S. Chen, *et al.*, "Surface Plasmon Resonance Biosensor Based on Smart Phone Platforms," Sci. Rep. **5**(1), 12864 (2015).
17. S. Nootchanat, W. Jaikeandee, P. Yaiwong, *et al.*, "Fabrication of Miniature Surface Plasmon Resonance Sensor Chips by Using Confined Sessile Drop Technique," ACS Appl. Mater. Interfaces **11**(12), 11954–11960 (2019).
18. E. Kretschmann and H. Raether, "Notizen: Radiative Decay of Non Radiative Surface Plasmons Excited by Light," Zeitschrift für Naturforschung A **23**(12), 2135–2136 (1968).
19. A. Otto, "Excitation of nonradiative surface plasma waves in silver by the method of frustrated total reflection," Z. Phys. A: Hadrons Nucl. **216**(4), 398–410 (1968).
20. H. Raether, *Surface Plasmons on Smooth and Rough Surfaces and on Gratings* (Springer-Verla, 1988).
21. S. Deng, P. Wang, and X. Yu, "Phase-Sensitive Surface Plasmon Resonance Sensors: Recent Progress and Future Prospects," Sensors **17**(12), 2819 (2017).
22. C. Odacı and U. Aydemir, "The surface plasmon resonance-based fiber optic sensors: A theoretical comparative study with 2D TMDC materials," Results in Optics **3**, 100063 (2021).
23. P. K. Maharana and R. Jha, "Chalcogenide prism and graphene multilayer based surface plasmon resonance affinity biosensor for high performance," Sens. Actuators, B **169**, 161–166 (2012).
24. A. A. Rifat, G. A. Mahdiraji, R. Ahmed, *et al.*, "Copper-Graphene-Based Photonic Crystal Fiber Plasmonic Biosensor," IEEE Photonics J. **8**(1), 1–8 (2016).
25. I. Tanabe, Y. Y. Tanaka, K. Watari, *et al.*, "Enhanced Surface Plasmon Resonance Wavelength Shifts by Molecular Electronic Absorption in Far- and Deep-Ultraviolet Regions," Sci. Rep. **10**(1), 9938 (2020).
26. E. Fontana, "Thickness optimization of metal films for the development of surface-plasmon-based sensors for nonabsorbing media," Appl. Opt. **45**(29), 7632–7642 (2006).
27. J. Jing, K. Liu, J. Jiang, *et al.*, "Performance improvement approaches for optical fiber SPR sensors and their sensing applications," Photonics Res. **10**(1), 126–147 (2022).
28. K. Kurihara, K. Nakamura, and K. Suzuki, "Asymmetric SPR sensor response curve-fitting equation for the accurate determination of SPR resonance angle," Sens. Actuators, B **86**(1), 49–57 (2002).
29. Z. Xia, F. Chu, Z. Bian, *et al.*, "Study of Surface Plasmon Resonance Sensor Based on Polymer-Tipped Optical Fiber With Barium Titanate Layer," J. Lightwave Technol. **38**(4), 912–918 (2020).
30. M. Mahabubur Rahman, M. Aslam Molla, A. Kumar Paul, *et al.*, "Numerical investigation of a highly sensitive plasmonic refractive index sensor utilizing hexagonal lattice of photonic crystal fiber," Results Phys. **18**, 103313 (2020).
31. Y. Guo, J. Li, S. Li, *et al.*, "Dual-polarized optical sensing of microstructure fiber with pentagonal-lattice based on surface plasmon resonance in the near-IR spectrum," Optik **202**, 163671 (2020).

Optics EXPRESS

32. Q. Wang, X.-Z. Wang, H. Song, *et al.*, "A dual channel self-compensation optical fiber biosensor based on coupling of surface plasmon polariton," Opt. Laser Technol. **124**, 106002 (2020).
33. A. Zuhayer, M. Abd-Elnaby, S. H. Ahammad, *et al.*, "A Gold-Plated Twin Core D-Formed Photonic Crystal Fiber (PCF) for Ultrahigh Sensitive Applications Based on Surface Plasmon Resonance (SPR) Approach," Plasmonics **17**(5), 2089–2101 (2022).